Single-Molecule Optoelectronics

TAE-HEE LEE,[†] JOSE I. GONZALEZ,
JIE ZHENG, AND ROBERT M. DICKSON*

School of Chemistry and Biochemistry, Georgia Institute of Technology, Atlanta, Georgia 30332-0400

Received June 1, 2004

ABSTRACT

With discrete states, several-atom Ag_n nanoclusters exhibit molecule-like behavior with strong visible fluorescence and robust optical properties. This new class of single-molecule fluorophores has been created and electrically contacted in thin films to produce the first electroluminescent single molecules. A direct reporter of nanoscale charge injection and transport through discrete energy levels, bright Ag_n electroluminescence has been harnessed to create single-molecule light-emitting diodes (LEDs) and optoelectronic logic gates and even to demonstrate full addition operations. These experiments utilizing the small size and quantum behavior of individual Ag nanoclusters usher in the new field of single-molecule optoelectronics.

Introduction

Exhibiting exquisite environmental sensitivity, single-molecule spectroscopy was first demonstrated at cryogenic temperatures,[1–3] but these quickly exploded with myriad room-temperature applications.[4–9] Although manifested very differently at room temperature due to greatly increased spectral broadening, similar environmental sensitivity persists and has enabled a wide range of experiments probing nanoscale dynamics.[3,5,9–13] The ever-expanding range of experimental observables matured from spectral shifts to encompass blinking,[9] three-dimensional orientational dynamics,[14] lifetime alterations,[11] and even photon-by-photon statistical analysis[15]

Tae-Hee Lee received his B.S. and M.S. degrees from Sogang University in Seoul, Korea, and his Ph.D. from the Georgia Institute of Technology. He is currently a postdoctoral scholar in Prof. Steven Chu's group at Stanford University. His research interests are in single-molecule dynamics and nanoscale energy and charge transport.

Jose I. Gonzalez is a native of Barranquilla, Colombia. He received B.S. degrees in chemistry and mathematics from the Massachusetts Institute of Technology in 2001 and is currently pursuing his Ph.D. at the Georgia Institute of Technology. His research interests are in the interplay between the electrical and optical properties of nanoscale species.

Jie Zheng obtained his B.S. and M.S. degrees from Inner Mongolia University and is currently pursuing his Ph.D. at the Georgia Institute of Technology. His research interests are in the optical and electronic properties of nanoscale metals along the atom to nanoparticle transition.

Robert M. Dickson received his B.A. from Haverford College in 1991 and his Ph.D. from the University of Chicago with Prof. Takeshi Oka in 1996. He spent 2 years as a postdoctoral fellow in W. E. Moerner's lab at UC–San Diego. He joined the School of Chemistry and Biochemistry at Georgia Tech in July 1998, where he is currently an Associate Professor. Dr. Dickson is a Camille and Henry Dreyfus Teacher–Scholar and an Alfred P. Sloan Fellow, and was named the Blanchard Assistant Professor of Chemistry in 2001. He is active in the fields of single-molecule microscopy, nanoscale metal optical properties and nanoscale charge injection and electroluminescence.

to extract subensemble information on a wide range of physical, chemical, and biological systems.

In most cases, the finite lifetime and rapid photobleaching of even the best chromophores used limit single-molecule sensitivities on both short and long time scales. Photon-by-photon statistical analyses have ameliorated some concerns at short times, but fundamentally, the several nanosecond radiative lifetimes and $\sim 10^{-16}$ cm^2 absorption cross sections limit emission rates even at high (e.g., kW/cm^2) incident laser intensities. Since photons convey information about single molecules and their environments, the radiative lifetimes must decrease and absorption cross sections increase to simultaneously create brighter fluorophores and be able to obtain fast time information. The long time information is similarly limited by irreversible photobleaching. Because good single molecule dyes typically emit only $\sim 10^7$ photons before photobleaching, both observation time and time resolution remain constrained.

While great advances have been made in following the dynamics of increasingly complex systems, our goal has been to move beyond using single molecules merely as probes of other heterogeneous systems and, instead, to develop true single-molecule optoelectronics.[16] Such electroluminescent single molecules should take advantage of the extremely small size and quantum behavior of electrically excited individual emitters.[17,18] However, to create high brightness and long-lived single-molecule optoelectronics, new ultrastable emitters with fast radiative lifetimes must be developed that efficiently emit when bridging nanoscale electrodes.

Strongly Fluorescent Noble Metal Nanoclusters

To accomplish our goals, we have created quantum-confined free electron metals that behave as a new class of artificial atoms with size-tunable optical properties in solutions and on oxide surfaces.[19–23] Devoid of a bulk band gap, size-tunable metal nanoclusters must be closer to the atomic scale and, therefore, much smaller than semiconductors to show discrete energy levels. Creating metal nanoclusters inherently requires understanding the atom to nanoparticle transition encompassing "molecular-scale metals". Such molecular metals retain their discrete energy levels with highly polarizable and potentially strongly fluorescent transitions between them. Silver and gold, for example, exhibit unique emission energy scalings due to the outermost electrons from each noble metal atom being delocalized within both the ground and excited states to enable transitions between discrete states within the nanocluster conduction band.[20,22,24–28] Size-dependent effects are then only observable when the free electrons are confined relative to the Fermi wavelength (~ 1 nm) of

* To whom correspondence should be addressed. E-mail: dickson@chemistry.gatech.edu.
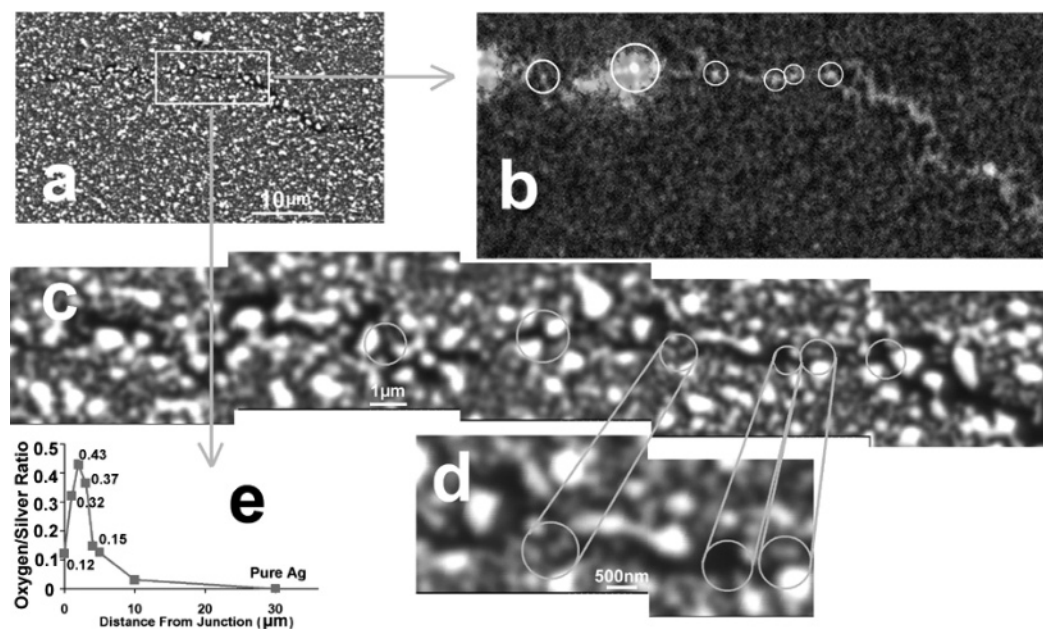† Current address: Department of Physics, Stanford University, Stanford, CA 94305.

FIGURE 1. Microscopic images of a silver nanocluster junction: (a) scanning electron micrograph (SEM, Hitachi S-3500H, 15 keV electron energy) of a typical silver nanocluster junction; (b) optical image (0.2-s CCD exposure collected with a 1.4 NA, 100× oil-immersion objective) from the region bounded by the white box in panel a. White circles represent the electroluminescent areas corresponding to those further magnified in the SEM images (panels c and d). Formed in situ by DC excitation, AC-excited emission (163 MHz sine wave with 5 V_{pp} ($\pm$2.5 V) amplitude) arises from species too small to be observed with SEM (<5 nm). Panel e shows the degree of oxidation with distance from the junction as determined with energy-dispersive spectroscopy (EDS, ThermoNoran attached to Hitachi S-3500H) from 3-μm diameter regions.

electrons in the nanocluster conduction band. Because of shell-filling degeneracies, transition energies scale *linearly* with the inverse cluster radius (R^{-1}) as predicted by the delocalized spherical free-electron model,[23,29−32] making these multielectron artificial atoms.

The well-defined geometries and low density of states of small noble metal nanoclusters produce molecule-like electronic energy levels. Experimentally, gas phase and low-temperature matrix-isolated silver nanoclusters exhibit discrete absorption and fluorescence and well-defined ionization potentials.[25,28,33−38] The geometries and discrete energy levels of these several-atom nanoclusters can also be calculated with reasonable accuracy.[39,40] Silver trimer, for example, has a global potential energy minimum with slightly distorted isosceles triangular geometry. Many small silver nanoclusters (Ag_2−Ag_4, Ag_8) exhibit strong visible fluorescence, which when combined with their photostability can be very useful in many photonics and optoelectronics applications. It is very likely that Ag_5, Ag_6, and Ag_7 also have visible fluorescence because their absorption spectra are also in the visible range. Larger nanoclusters (Ag_N, $N \geq 10$) can absorb yellow-red light and may provide additional tunability into the red or near-IR[33]

Single-Molecule Optoelectronics of Silver and Gold Nanoclusters

Molecular electronics has become adept at creating nanoscale junctions,[16,41−43] although reproducibility is often a cause for great concern.[44] Two-electrode nanoscale junctions are readily formed, however, by making very thin wires spanning larger electrodes and either mechani-

cally[41] or electrically[16,45] breaking the narrow connection. Mechanically breaking electrodes can be performed through deforming the substrate on which the electrodes are fabricated and should yield true homojunctions, if done symmetrically. While quite straightforward, this method is rather difficult to implement and leaves presumably metallic electrodes to contact the molecule of interest. Electrical methods of causing electrode separation actually induce chemical transformations at the most resistive (narrowest) region. Occurring through electromigration, momentum is transferred from electrons to the heavier silver atoms. This asymmetric process moves material from the cathode to the anode and eventually forms a catastrophic break separating the two electrodes.[46−48] While such electrodes are often considered homojunctions with metallic contacts, scanning electron microscopy confirms that the electrodes actually become asymmetrically oxidized during the DC electromigration process (Figure 1).[17,49] These semiconducting electrodes are capable of preserving the discrete energy levels of contacted molecules due to their noncontinuous density of states[50] and contribute to observed asymmetries in the nanoscale junction electrical properties.

Likely an important consideration in molecular electronics experiments, small numbers of few-atom metal nanoclusters are also left behind within the nanoscale break junctions. These nanoscale features have optical properties nearly identical to those we create in solution[19] and act as molecular-scale tunneling bridges connecting the two electrodes to simultaneously conduct charge and electroluminesce. Because of the asymmetric DC fabrication process, the energy levels of these nanoclusters are
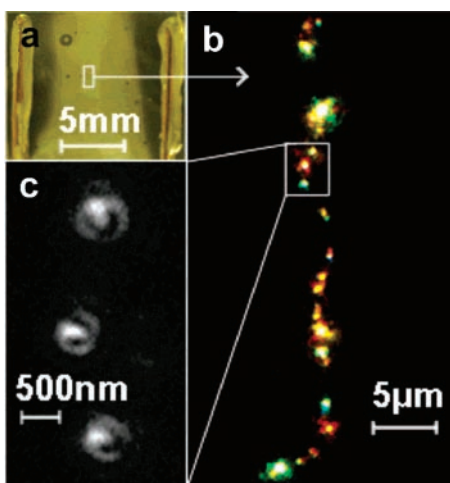
FIGURE 2. Single silver nanocluster electroluminescence: (a) discolored Ag_2O region between copper electrodes on a glass substrate in a vacuum ($\sim10^{-5}$ Torr) with 9 V DC potentials applied across the film; (b) multicolored electroluminescence from single Ag_n ($n = 2-8$) molecules occurs within the electrically discolored region; (c) these features exhibit dipole emission patterns and blinking dynamics (not shown) characteristic of single-molecule behavior.

more closely tied to those of the anode[49]—the primary cause of asymmetry in device operation. One-dimensional arrays of various metal nanoclusters are readily formed electrically within thin metal films through this facile electromigration process. Though demonstrated for Ag,[16,51,52] Au,[53] and Cu,[16,54] we will limit our discussion to the representative case of Ag nanocluster electroluminescence (EL).

Silver Nanocluster Single-Molecule Electroluminescence. When a DC electric field is applied to the electromigration-induced silver oxide nanogap junctions, strong electroluminescence is observed from many spatially resolved individual silver nanoclusters (Figure 2).[16] The DC electroluminescence of all nanoclusters in the junction spans the entire visible spectrum. The overall spectra shift toward higher energy with increasing applied voltage (Figure 3).[16] Even the DC-excited electroluminescence emission spectra of individual nanoclusters are quite broad due to the chemical, thermal, and electrical strains on the silver nanoclusters under such high current and field strength (Figure 4). The correlated peaks in EL and current flow arise from charge flow through but rapid thermal destruction of the junction, thereby limiting practical EL experiments to about 15 min (Figure 3). Despite the instability, emissive spots show evidence of single-molecular emission such as on/off blinking and dipolar emission patterns (Figure 2).

Formed junctions show very stable and strong emission under AC electric fields that match the RLC (resistance-inductance-capacitance) resonance of ~160 MHz. The efficiency with AC excitation is often 4 orders of magnitude higher than that with DC. In contrast to the DC spectra, individual electroluminescent silver nanoclusters that show broad emission under DC excitation exhibit very narrow spectra under AC excitation (Figure 4) indicating that the transitions between well defined local states yield
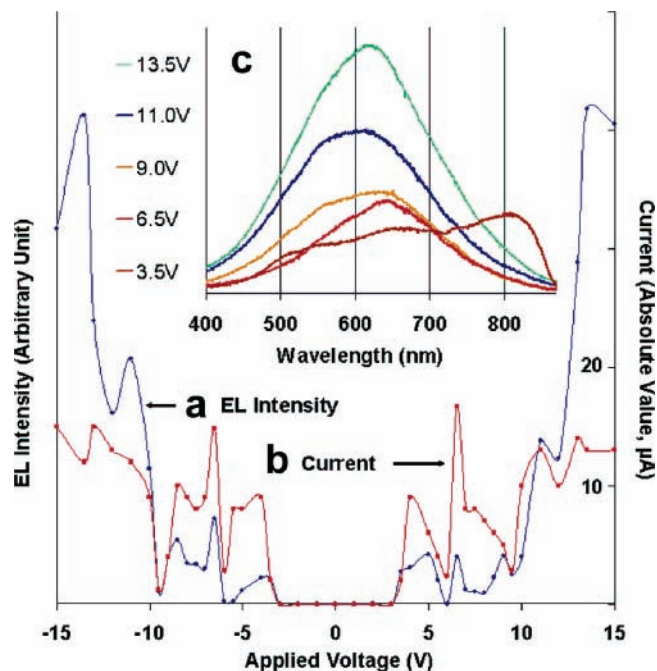

FIGURE 3. Typical voltage-dependent (a) electroluminescence (EL) intensity from and (b) concomitant absolute value of current flow through all species within the 100-μm field of view. Peaks in the emission intensity vs applied voltage curve result from preferential electron extraction from and subsequent re-injection into subsets of specifically sized and shaped Ag_n molecules. The absolute voltages at which these peaks occur depend slightly on junction formation with electroluminescence onset occurring between 3.5 and 5 V. These processes result in the correlated conduction and subsequent electron–hole recombination within Ag nanoclusters. Independent of field polarity and ground level, this must be field-induced conduction and electroluminescence. Part c shows the electroluminescence spectra (30-s CCD exposures, 0.30-m monochromator) corresponding to selected data points in parts a and b. As applied DC voltage is increased, lower energy features burn out because of Joule heating resulting in peaks in parts a and b and the corresponding spectral shifts to higher frequencies.

strong EL. Thus, AC excitation yields highly stable fluorescence-like electroluminescence by injecting charge at the optimal times and reducing thermal decay of the silver nanocluster excited states.

Single-Molecule Electroluminescence Mechanism. Using the junction elemental analysis and the bridging Ag nanocluster spectral properties, we constructed a junction energy level diagram using published experimental and theoretical values for the absolute energies of all materials (Figure 5).[38–40,55] As revealed by microscopic analysis, the junction silver nanoclusters are separated from the electrodes to yield a tunneling barrier that should preserve the discrete nanocluster energy levels.

Since the DC EL intensity does not show any noticeable polarity dependence (Figure 3), electroluminescence likely arises from a two-step process: field ionization (hole injection), followed by electron re-injection into the nanocluster excited state, with subsequent radiative recombination. With such strong fields applied ($\sim10^9$ V/m), holes are injected into silver nanoclusters within the junction, and electrons can be resonantly re-injected into excited states through field emission from the electrodes.
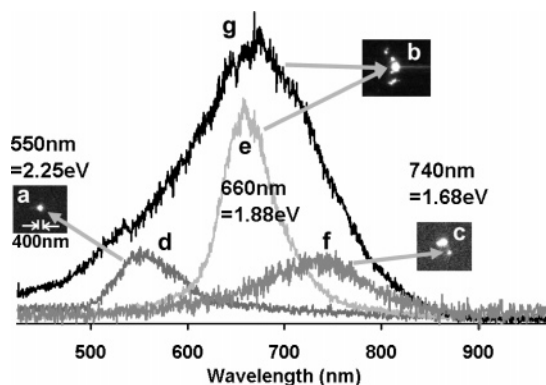
FIGURE 4. AC- and DC-excited single-molecule electroluminescence spectra. Emission from spatially resolved individual molecules was imaged through a 300-mm imaging monochromator (Acton) with a mirror in place of the grating. Slit width, position, and CCD region of interest were adjusted such that upon rotation of a 150 lines/mm grating into the path, single-molecule spectra are readily obtained. Single molecule images (a,b,c) have corresponding AC-excited (160 MHz, ±2 V) electroluminescence spectra d, e, and f, respectively, with emission maxima at 550, 660, and 740 nm (15-s integration). All AC-excited spectra are very stable. Spectrum f is magnified (3×) so that the peak can be clearly seen. The same nanocluster that yields spectrum e under AC excitation yields spectrum g under 7 V DC excitation, the voltage necessary to yield comparable EL intensity. Clearly, DC-excited emission is much broader due to fast spectral dynamics resulting from severe chemical changes in the nanocluster, which end up destroying it after several minutes.
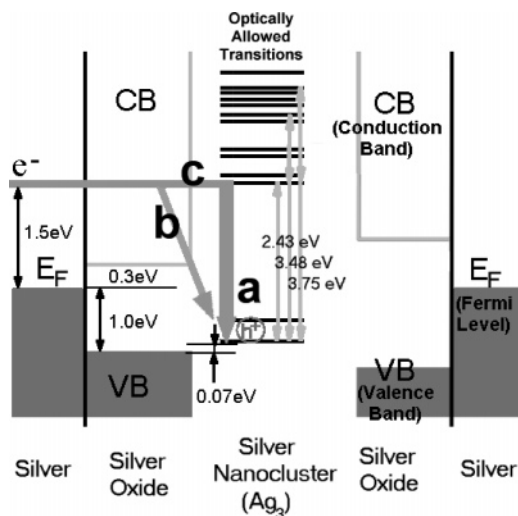

FIGURE 5. Composite energy diagram governing silver nanocluster electroluminescence. The photoelectric work function of Ag(111) (4.74 eV), X-ray and inverse photoelectron spectroscopy of the Ag_2O band structure,[55] gas-phase ionization potential (5.66 eV),[38] and calculated electronic energy levels[39,40] of Ag_3 are all plotted on the same energy scale to illustrate electroluminescence from silver trimer. Other small nanoclusters also have both visible emission and molecular energy levels favorable for EL in this device geometry.[38] Holes can be trapped in silver nanoclusters because their energies lie within the oxide band gap. In step a, after the hole is formed by field extraction, election re-injection causes either (b) nonradiative thermal decay or (c) excited-state injection with subsequent emission. Optimal hole formation and electron re-injection times are found to range between 2.8 and 3.5 ns from two-pulse excitation experiments.

Resulting from HOMO levels of several nanoclusters being within the band gap of the semiconducting Ag_2O electrode

surface, such ionized silver nanoclusters can be quite stable even at room temperature. The combination of a tunneling gap and semiconducting electrodes simultaneously limits energy level broadening and enables positively charged Ag nanoclusters to survive until neutralized through electron re-injection into the excited states, thereby producing electroluminescence when they radiatively decay. The energy levels of this $Ag/Ag_2O/Ag_n/Ag_2O/$ Ag system are very nicely aligned to trap electron–hole pairs and produce EL.

To simultaneously investigate mechanistic details and minimize thermal destruction, high-frequency AC/two-pulse excitation was employed to excite the nanoclusters and probe their time-dependent electroluminescent response. The polarity, interpulse delay, pulse widths, and pulse amplitudes were all independently controlled experimental variables within a composite two-pulse sequence.[17,18] The total EL intensities from all nanoclusters within each junction depend on the different set of pulse variables—hole injection time/energy (first pulse width/ amplitude), hole lifetime (interpulse delay), and electron re-injection time/energy (second pulse width/amplitude). Maximal bulk Ag_n EL is observed with a 3.0-ns first pulse, a 3.3-ns second pulse, and a 3.2-ns interpulse delay.[18]

Single Nanocluster Light-Emitting Diodes (LEDs) and EL Excitation Spectra. Although the EL process appears to be polarity-independent under DC and AC electrical excitation (e.g., Figure 3), separation of the charge injection processes via pulsed excitation shows clear asymmetry.[17,18] For a given set of inputs, the responses of spatially resolved individual electroluminescent nanoclusters can be directly read to elucidate their distinctive EL characteristics. The individual nanocluster responses differ significantly from that of the ensemble (Figure 6).[17] Consistent with the suggested EL mechanism of hole injection with the first pulse followed by electron re-injection with the second pulse, these peaks in the EL intensity should correlate with injection into the silver nanocluster excited states. Because the nanocluster energy levels are more closely tied to those of the anode, a negative second pulse must be used to inject electrons into the nanocluster excited states to yield EL. Consequently, only positive followed by negative pulses injected into the anode produce electroluminescence.[18] This asymmetry and LED behavior results from the heterojunction nature and the preferential coupling of nanocluster energy levels to the anode and is also clearly evident in photoconductivity experiments when exciting individual nanoclusters within the junctions.[49] Only observable when separating the charge injection steps, this inherent asymmetry results from the directional DC fabrication process.

Consistent with our understanding of single-molecule electroluminescence, the EL intensity should be proportional to the tunneling current from the electrode to the excited states of silver nanoclusters, provided that the first pulse is first applied for hole injection. As the quasi-Fermi level of the anode increases with increased second pulse amplitude, more channels for charge re-injection become available through the silver nanocluster excited states as
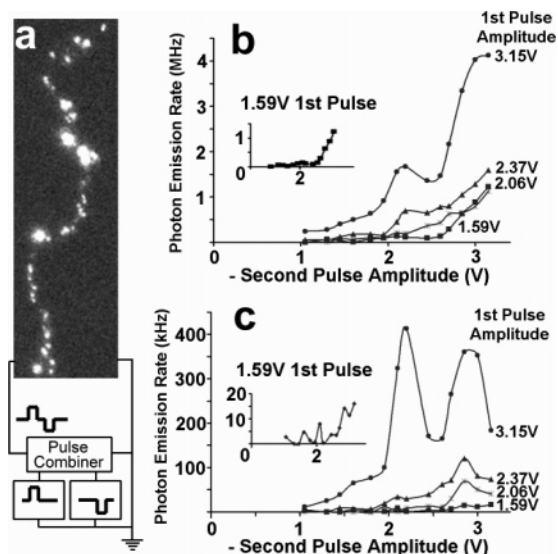
FIGURE 6. Quantum optoelectronic characteristics of typical Ag nanocluster junctions. Panel a shows a typical Ag$_n$ electroluminescent region with two consecutive pulse excitation (25 MHz repetition rate) exhibiting blinking and dipole emission patterns characteristic of individual molecules. The EL shows a strong pulse polarity dependence and is detected only with a positive followed by a negative pulse with proper widths (2−4 ns), amplitudes, and interpulse delay (<4 ns). Other two-pulse polarity combinations yield no detectable emission. The EL intensity also depends strongly on the amplitudes of the positive first and negative second pulses. In panel b, integrated EL from ∼30 molecules exhibits nearly monotonically increasing emission with both first and second pulse amplitudes. Positive pulses 4 ns ahead of the negative pulses, each with 2.6 ns pulse widths and 1.0 ns transition times, were used. On/off ratios of 15 were obtained with −2.1 V signal pulses (the second pulse) following either 1.59 V (Off) or 3.15 V (On) gate pulses. The inset expands the lowest voltage case, showing the threshold behavior. In panel c, integrated emission from five similar molecules exhibits three clear peaks along the second pulse amplitude at −1.6, −2.1, and −2.85 V.

given by Landauer conduction.[56] The peaks in the dI_{EL}/d$V_{\text{second pulse}}$, therefore, should match the absorption spectra of the silver nanoclusters. However, in our system, the inelastically tunneling electrons have a narrow energy distribution because they are most likely field emitted; the nanoclusters are separated from the electrodes by a tunneling gap and semiconducting silver oxide layer (Figure 7).[57,58] Therefore, the electroluminescence intensity is directly proportional to the overlap of the narrow electron energy distribution and the silver nanocluster excited states. The electron energy distribution can be approximated from the Fowler−Nordheim description of field emission.[59] The very narrow tunneling electron energy distributions exhibit scattering structures due to the discrete energy levels of surface adsorbates.[57,58,60−62] As shown in Figure 7, with applied voltage V, the voltages producing quasi-Fermi levels expected to give a net current from the anode to silver nanoclusters range from $E_f − eV/2$ to $E_f + eV/2$ assuming the two electrodes comprise opposing parallel metal plates with constant densities of states (DOS). Since the electrodes are nearly metallic, the rate of electron transfer or transition between the nanoclusters and the electrodes is also assumed to
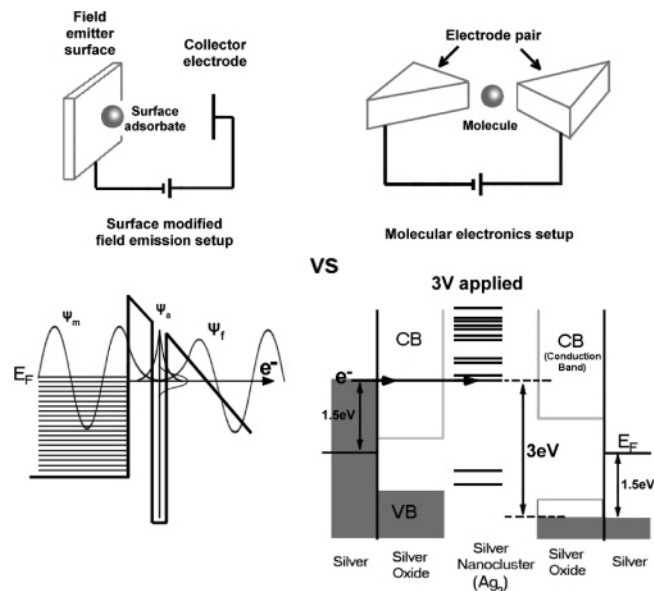

FIGURE 7. Comparison between field emission experiments and molecular electronics experiments. The field strengths used in molecular electronics experiments are high enough to cause field emission ($10^8 − 10^9$ V/m). The current level observed in many molecular electronics experiments ($10^{-6} − 10^{-14}$ A) is also comparable to that of many field emission cases. Lower left panel shows the elastic tunneling of an electron with the metal electronic wave function (ψ_m) facilitated by the surface state (ψ_a) introduced by a surface-adsorbed molecule.[57] The energy distribution of the field-emitted electrons or the tunneling electronic wave function (ψ_f) often reveals the surface states. Inelastic tunneling revealing surface vibrational structure has also been seen in the field-emission geometry.[57,60,65] Therefore, based on the similarity (both in quantitative and qualitative considerations) between the two cases shown here and within typical molecular electronics geometries, the tunneling current through the molecules as a function of the electron energy will likely reflect the energy levels of the molecules as shown in Figure 5. By application of 3 V across the molecule in this nanoscale device, an energy difference of 1.5 eV is created between each electrode and Fermi level.

be constant. By integrating the product of the field-emitted energy distribution and the DOS of silver nanoclusters over the range of $E_f − eV/2$ to $E_f + eV/2$, one can estimate the tunneling probability of field-emitted electrons through the excited silver nanocluster states, thereby yielding the EL intensity.[51,57] Comparing electron injection/electroluminescence excitation spectra with the calculated absorption spectra of Ag$_2$−Ag$_8$,[39,40] the simulated I_{EL} vs V characteristics with Ag$_3$, Ag$_5$, and Ag$_6$ are found to closely match the experimental EL intensities from different nanoclusters (Figure 8). The relative position of E_f with respect to the silver nanocluster HOMO energy levels cannot be determined solely from theory due to the high degree of local geometry variation surrounding the individual nanoclusters. Such local corrections will greatly modify the local work function and shift the absolute excitation peak positions,[50,51,57] but the relative positions should remain unchanged. The simulations, however, indicate that the peaks in EL intensity should match the peaks of the silver nanocluster absorption spectra with an offset not exceeding the nanocluster HOMO−LUMO gap (2−3 eV).[25,27,28,33,63]
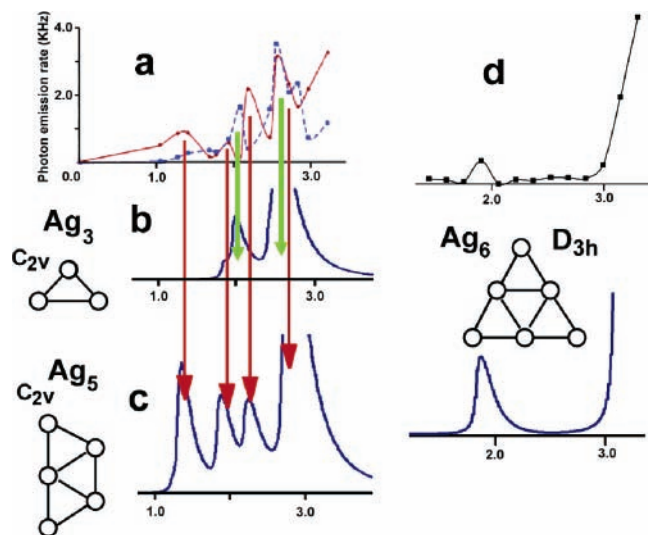
FIGURE 8. Single silver nanocluster electroluminescence reveals detailed electronic structure. In panel a, two electroluminescent nanoclusters show discrete on/off behavior with varying second pulse (electron re-injection pulse) amplitude indicative of their excited electronic states. Panels b and c reveal that the two nanoclusters in panel a are likely Ag_3 and Ag_5 based on their calculated excited electronic states. In panel d, another electroluminescent nanocluster is likely to be Ag_6. Arbitrary but reasonable offset of the energy (<2 eV) is used to match the signature of the on/off behavior to the energy states to reflect the heterogeneity of the junction and variation of local work function controlling injection into each nanocluster.

Single-Molecule Electroluminescence-Based Opto-electronic Logic Gates. Because electroluminescence is a direct reporter of current flow, we can simultaneously utilize these subnanometer emitters as quantum mechanical light sources and as readouts to understand charge injection and transport on the nanoscale. The single-entity nature of these noble metal nanocluster emitters was recently demonstrated through antibunched electroluminescence[53] and opens new opportunities in single-photon sources and nanophotonics. Additionally, the injection into and conduction through discrete Ag nanocluster energy levels yields complex negative differential resistance-like on/off behavior of silver nanocluster EL.[17] Representative of nanoscale charge flow but much easier to measure, the voltage-dependent EL can potentially be used to improve electronic circuit efficiency.[17] Compared to current field effect transistor (FET)-based electronic circuits that rely on the two state switching schemes, complex switching can yield much more compact electronics by providing a way to engineer the same function with many fewer switching elements.[17] As an example, Ag_3 and Ag_5 molecules can individually act as AND and XOR gates, respectively (Figure 9) by injecting charge at well-defined voltages. Although the output is light instead of current, the output EL intensity is a direct probe of current passing through the junction nanoclusters. Furthermore, a full adder employing only two individual molecules (one Ag_3 and one Ag_5 in a complex logic sequence cascade adding three input bits to produce two output bits) was implemented.[17] The demonstrated full adder example shows reasonably good on/off ratios ranging from 6.0 to 12.2
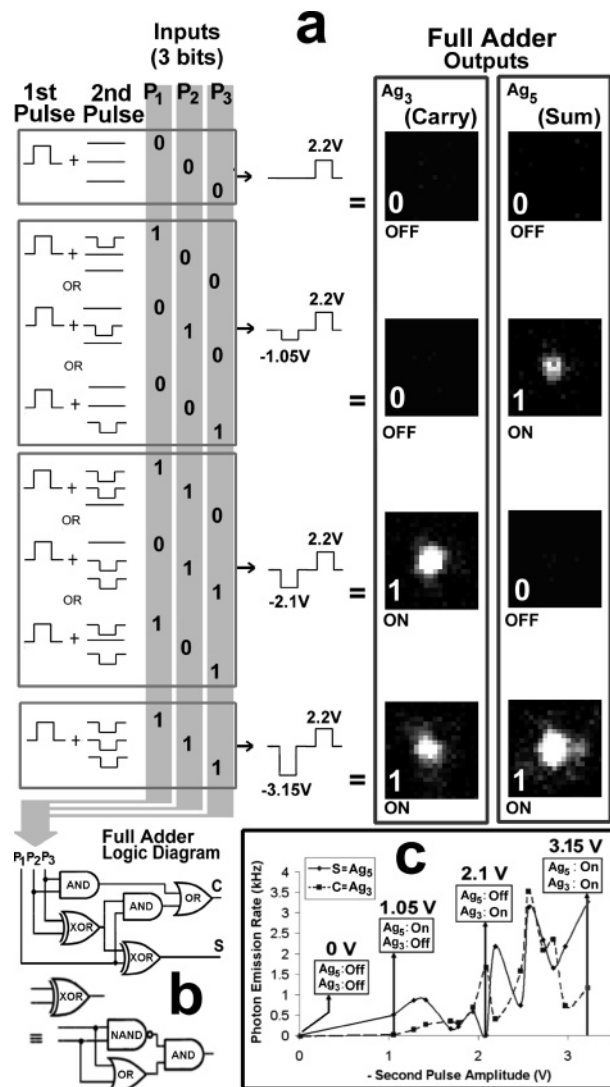

FIGURE 9. Quantum optoelectronic logic operations with coupled individual silver nanoclusters at room temperature. In panel a, with the use of 2.6 ns pulses at 25 MHz repetition rates, a 2.2 V first pulse was always added prior to the second composite pulse, which itself was constructed from three separate input pulses (P_1, P_2, P_3), each with either 0.0 or −1.05 V amplitude. Voltages described below refer to the composite second pulse amplitudes. In panel b, nanocluster Ag_5 is turned on ("1") at −1.05 and −3.15 V and turned off ("0") at −2.1 V. Nanocluster Ag_3 is turned on at −2.1 and −3.15 V and turned off at −1.05 V. When only two input pulses with 0 V (="0") or −1.05 V (="1") amplitude are used, Ag_5 and Ag_3 act as XOR and AND gates, respectively, to constitute a half adder. For example, if only P_2 and P_3 are used as inputs, C (EL on/off state of Ag_3) = ((P_2 OR P_3) AND NOT (P_2 AND P_3)) and S (EL on/off state of Ag_5) = (P_2 AND P_3). The on/off ratios for XOR and AND molecules are 6.0 and 12.2, respectively. The same molecules can also be fed with three inputs to work as a full adder. Input pulses and results for arithmetic addition of the corresponding three bits are shown in panel a. In panel c, the discrete EL-producing energy levels of these two nanoclusters enable operation as a full adder. Nanoclusters Ag_5 and Ag_3 act as the output nodes in the logic diagram incorporating nine basic binary logic gates typically requiring at least 25 standard field effect transistors. In the full adder implementation demonstrated in panel a, EL on/off state of nanocluster Ag_5 = ((P_2 XOR P_3) XOR P_1) and EL on/off state of Ag_3 = (P_1 AND (P_2 XOR P_3)) OR (P_2 AND P_3), in which XOR is defined as: a XOR b = ((a OR b) AND NOT (a AND b)).

(Figure 9). One can potentially build true optoelectronic circuits by conveying the EL outputs of the logic operations to the next silver nanoclusters utilizing the photoconductivity of the nanoclusters.[49] Therefore, by utilizing the complex on/off behavior of the single-molecular EL based on the inelastic electron tunneling through discrete electronic states of individual nanoclusters, one can potentially build highly compact, complex optoelectronic circuits,[17,49,64] for example, a full adder employing two silver nanoclusters instead of at least 25 normal FETs.

Giving rise to the Ag EL brightness, the extremely fast, ~30 ps Ag lifetime makes definitive proof of single-molecule emission through antibunching observations very challenging. Au, however, exhibits more tractable ~500 ps EL lifetimes that enabled our recent demonstration of antibunched Au nanocluster EL directly confirming the single-entity nature of these nanogold emitters.[53] No visible EL emanates from Au, which only emits in the useful near-IR region. This IR electroluminescence could be very useful for telecommunications applications such as quantum encryption through currently available optical fibers. The order of magnitude difference in the excited-state lifetime between gold and silver nanodots makes them complementary and simultaneously attractive to future nanoscale optoelectronic applications as electrically driven single-photon sources.

Conclusion

Although currently limited by fluorophore optical properties, room-temperature single-molecule/nanoparticle spectroscopy is cementing its role as an indispensable tool for unraveling the dynamics within heterogeneous biological and materials systems. We have created "molecular metals"—several atom noble metal nanoclusters—as new fluorophores with greatly improved fluorescent properties. Created both in solution[19−21,23] and within thin films,[16,22,53] these noble metal nanoclusters behave as subnanometer single-quantum systems that are being explored as active individual optoelectronic elements in single-molecule electroluminescent structures. The quantum electronics built on individual nanoclusters has even yielded a full adder using light as the output. Since electroluminescence is a reporter of current flow but single photons are much more easily measured than are single electrons, these electroluminescent nanoclusters provide a noncontroversial and corroborative readout of nanoscale current flow. With further engineering, it is hoped that electrodes can be designed to make a much wider range of inorganic and molecule-like species electroluminesce as individual entities with well-defined discrete states.

References

(1) Moerner, W. E.; Kador, L. Optical detection and spectroscopy of single molecules in a solid. *Phys. Rev. Lett.* **1989**, *62*, 2535−2538.

(2) Orrit, M.; Bernard, J. Single pentacene molecules detected by fluorescence excitation in a p-terphenyl crystal. *Phys. Rev. Lett.* **1990**, *65*, 2716−2719.

(3) Reilly, P. D.; Skinner, J. L. Spectral diffusion of single molecule fluorescence: a probe of low-frequency localized excitations in disordered crystals. *Phys. Rev. Lett.* **1993**, *71*, 4257−4260.

(4) Xie, X. S. Single-Molecule Spectroscopy and Dynamics at Room Temperature. *Acc. Chem. Res.* **1996**, *29*, 598−606.

(5) Trautman, J. K.; Macklin, J. J. Time-resolved spectroscopy of single molecules using near-field and far-field optics. *Chem. Phys.* **1996**, *205*, 221−229.

(6) Ha, T.; Zhuang, X.; Kim, H. D.; Orr, J. W.; Williamson, J. R.; Chu, S. Ligand-induced conformational changes observed in single RNA molecules. *Science* **1999**, *96*, 9077−9082.

(7) Bartko, A. P.; Dickson, R. M. Three-Dimensional Orientations of Polymer-Bound Single Molecules. *J. Phys. Chem. B* **1999**, *103*, 3053−3056.

(8) Fleury, L.; Segura, J. M.; Zumofen, G.; Hecht, B.; Wild, U. P. Nonclassical photon statistics in single-molecule fluorescence at room temperature. *Phys. Rev. Lett.* **2000**, *84*, 1148−1151.

(9) Dickson, R. M.; Cubitt, A. B.; Tsien, R. Y.; Moerner, W. E. On/off blinking and switching behaviour of single molecules of green fluorescent protein. *Nature* **1997**, *388*, 355−358.

(10) Moerner, W. E. Examining Nanoenvironments in Solids on the Scale of a Single, Isolated Molecule. *Science* **1994**, *265*, 46−53.

(11) Ambrose, W. P.; Goodwin, P. M.; Martin, J. C.; Keller, R. A. Alterations of single molecule fluorescence lifetimes in near-field optical microscopy. *Science* **1994**, *265*, 364−367.

(12) Nie, S.; Chiu, D. T.; Zare, R. N. Probing individual molecules with confocal fluorescence microscopy. *Science* **1994**, *266*, 1018−1021.

(13) Lu, H. P.; Xie, X. S. Single-Molecule Spectral Fluctuations at Room Temperature. *Nature* **1997**, *385*, 143−146.

(14) Bartko, A. P.; Xu, K.; Dickson, R. M. Three-dimensional single molecule rotational diffusion in glassy state polymer films. *Phys. Rev. Lett.* **2002**, *89*, No. 026101.

(15) Yang, H.; Xie, X. S. Statistical approaches for probing single-molecule dynamics photon-by-photon. *J. Chem. Phys.* **2002**, *117*, 10965−10979.

(16) Lee, T.-H.; Gonzalez, J. I.; Dickson, R. M. Strongly enhanced field-dependent single-molecule electroluminescence. *Proc. Natl. Acad. Sci. U.S.A.* **2002**, *99*, 10272−10275.

(17) Lee, T.-H.; Dickson, R. M. Two-terminal single nanocluster quantum optoelectronic logic gates. *Proc. Natl. Acad. Sci. U.S.A.* **2003**, *100*, 3043−3046.

(18) Lee, T.-H.; Dickson, R. M. Single-Molecule LEDs from Nanoscale Electroluminescent Junctions. *J. Phys. Chem. B* **2003**, *107*, 7387−7390.

(19) Zheng, J.; Dickson, R. M. Individual water-soluble dendrimer-encapsulated silver nanodot fluorescence. *J. Am. Chem. Soc.* **2002**, *124*, 13982−13983.

(20) Zheng, J.; Petty, J. T.; Dickson, R. M. High Quantum Yield Blue Emission from Water-Soluble Au_8 Nanodots. *J. Am. Chem. Soc.* **2003**, *125*, 7780−7781.

(21) Petty, J. T.; Zheng, J.; Hud, N. V.; Dickson, R. M. DNA-Templated Ag Nanocluster Formation. *J. Am. Chem. Soc.* **2004**, *126*, 5207−5212.

(22) Peyser, L. A.; Vinson, A. E.; Bartko, A. P.; Dickson, R. M. Photoactivated fluorescence from individual silver nanoclusters. *Science* **2001**, *291*, 103−106.

(23) Zheng, J.; Zhang, C.; Dickson, R. M. Highly Fluorescent, Water-Soluble, Size-Tunable Gold Quantum Dots. *Phys. Rev. Lett.* **2004**, *93*, No. 077402.

(24) Chen, S. W.; Ingram, R. S.; Hostetler, M. J.; Pietron, J. J.; Murray, R. W.; Schaaff, T. G.; Khoury, J. T.; Alvarez, M. M.; Whetten, R. L. Gold nanoelectrodes of varied size: Transition to molecule-like charging. *Science* **1998**, *280*, 2098−2101.

(25) Felix, C.; Sieber, C.; Harbich, W.; Buttet, J.; Rabin, I.; Schulze, W.; Ertl, G. Ag_8 Fluorescence in Argon. *Phys. Rev. Lett.* **2001**, *86*, 2992−2995.

(26) Rabin, I.; Schulze, W.; Ertl, G. Light emission during the agglomeration of silver clusters in noble gas matrices. *J. Chem. Phys.* **1998**, *108*, 5137−5142.

(27) Rabin, I.; Schulze, W.; Ertl, G. Absorption spectra of small silver clusters Ag-n (n >= 3). *Chem. Phys. Lett.* **1999**, *312*, 394−398.

(28) Felix, C.; Sieber, C.; Harbich, W.; Buttet, J.; Rabin, I.; Schulze, W.; Ertl, G. Fluorescence and excitation spectra of Ag-4 in an argon matrix. *Chem. Phys. Lett.* **1999**, *313*, 105−109.

(29) Knight, W. D.; Clemenger, K.; Deheer, W. A.; Saunders: W. A.; Chou, M. Y.; Cohen, M. L. Electronic Shell Structure and Abundances of Sodium Clusters. *Phys. Rev. Lett.* **1984**, *52*, 2141−2143.

(30) Haberland, H., Ed. *Clusters of Atoms and Molecules*; Springer Series in Chemical Physics, Vol. 52; Springer-Verlag: Berlin, 1994.

(31) Deheer, W. A. The Physics of Simple Metal-Clusters − Experimental Aspects and Simple-Models. *Rev. Mod. Phys.* **1993**, *65*, 611−676.

(32) Brus, L. E. Electron−Electron and Electron−Hole Interactions in Small Semiconductor Crystallites − the Size Dependence of the Lowest Excited Electronic State. *J. Chem. Phys.* **1984**, *80*, 4403−4409.

(33) Ozin, G. A.; Huber, H. Cryophotoclustering Techniques for Synthesizing Very Small, Naked Silver Clusters Ag_n of Known Size (Where $n=2-5$). The Molecular Metal Cluster-Bulk Metal Particle Interface. *Inorg. Chem.* **1978**, *17*, 155−163.

(34) Harbich, W.; Fedrigo, S.; Meyer, F.; Lindsay, D. M.; Lignieres, J.; Rivoal, J. C.; Kreisle, D. Deposition of mass selected silver clusters in rare gas matrices. *J. Chem. Phys.* **1990**, *93*, 8535−8543.

(35) Okazaki, T.; Saito, Y.; Kasuya, A.; Nishina, Y. Optical emission spectra of Ag_3 molecules in the gas evaporation technique. *J. Chem. Phys.* **1996**, *104*, 812−814.

(36) Harbich, W.; Fedrigo, S.; Buttet, J. The Optical-Absorption Spectra of Small Silver Clusters ($N = 5-11$) Embedded in Argon Matrices. *Chem. Phys. Lett.* **1992**, *195*, 613−617.

(37) Konig, L.; Rabin, I.; Schulze, W.; Ertl, G. Chemiluminescence in the agglomeration of metal clusters. *Science* **1996**, *274*, 1353−1355.

(38) Alameddin, G.; Hunter, J.; Cameron, D.; Kappes, M. M. Electronic and geometric structure in silver clusters. *Chem. Phys. Lett.* **1992**, *192*, 122−128.

(39) Bonacic-Koutecky, V.; Veyret, V.; Mitric, R. Ab initio study of the absorption spectra of Ag_n ($n=5-8$) clusters. *J. Chem. Phys.* **2001**, *115*, 10450−10460.

(40) Bonacic-Koutecky, V.; Cespiva, L.; Fantucci, P.; Koutecky, J. Effective core potential-configuration interaction study of electronic structure and geometry of small neutral and cationic Ag_n clusters: predictions and interpretation of measured properties. *J. Chem. Phys.* **1993**, *98*, 7981−7994.

(41) Reed, M. A.; Zhou, C.; Muller, C. J.; Brugin, T. P.; Tour, J. M. Conductance of a molecular junction. *Science* **1997**, *278*, 252−254.

(42) Klein, D. L.; McEuen, P. L.; Katari, J. E. B.; Roth, R.; Alivisatos, A. P. An approach to electrical studies of single nanocrystals. *Appl. Phys. Lett.* **1996**, *68*, 2574−2576.

(43) Park, J.; Pasupathy, A. N.; Goldsmith, J. I.; Chang, C.; Yaish, Y.; Petta, J. R.; Rinkoski, M.; Sethna, J. P.; Abruna, H. D.; McEuen, P. L.; Ralph, D. C. Coulomb blockade and the Kondo effect in single-atom transistors. *Nature* **2002**, *417*, 722−725.

(44) Service, R. F. Molecular Electronics: Next-Generation Technology Hits an Early Midlife Crisis. *Science*, **2003**, *302*, 556−559.

(45) Park, H.; Lim, A. K. L.; Alivisatos, A. P.; Park, J.; McEuen, P. L. Fabrication of metallic electrodes with nanometer separation by electromigration. *Appl. Phys. Lett.* **1999**, *75*, 301−303.

(46) Ho, P. S.; Kwok, T. Electromigration in metals. *Rep. Prog. Phys.* **1989**, *52*, 301−348.

(47) Schimschak, M.; Krug, J. Electromigration-Induced Breakup of Two-Dimensional Voids. *Phys. Rev. Lett.* **1998**, *80*, 1674−1677.

(48) Lloyd, J. R. Electromigration in integrated-circuit conductors. *J. Phys. D* **1999**, *32*, R109−R118.

(49) Lee, T.-H.; Hladik, C. R.; Dickson, R. M. Asymmetric Photo-conductivity within Nanoscale Break Junctions. *Nano Lett.* **2003**, *3*, 1561−1564.

(50) Basch, H.; Ratner, M. A. Binding at molecule/gold transport interfaces. I. Geometry and bonding. *J. Chem. Phys.* **2003**, *119*, 11926−11942.

(51) Nazin, G. V.; Qiu, X. H.; Ho, W. Atomic Engineering of Photon Emission with a Scanning Tunneling Microscope. *Phys. Rev. Lett.* **2003**, *90*, No. 216110.

(52) Nepijko, S. A.; Fedorovich, R. D.; Viduta, L. V.; Ievlev, D. N.; Schulze, W. Light emission from Ag cluster films excited by conduction current. *Ann. Phys. (Berlin)* **2000**, *9*, 125−131.

(53) Gonzalez, J. I.; Lee, T.-H.; Dickson, R. M. Quantum Mechanical Single-Gold-Nanocluster Electroluminescent Light Source at Room Temperature. *Phys. Rev. Lett.* **2004**, *93*, No. 147402.

(54) Nepijko, S. A.; Fedorovich, R. D.; Viduta, L. V.; Ievlev, D. N.; Schulze, W. Light emission from small copper particles excited by current passage or by low-energy electron bombardment. *Physica B* **2001**, *301*, 261−266.

(55) Tjeng, L. H.; Meinders, M. B. J.; Elp, J. V.; Ghijsen, J.; Sawatzky, G. A.; Johnson, R. L. Electronic Structure of Ag_2O. *Phys. Rev. B* **1990**, *41*, 3190−3198.

(56) Imry, Y.; Landauer, R. Conductance viewed as transmission. *Rev. Mod. Phys.* **1999**, *71*, S306−S312.

(57) Gadzuk, J. W.; Plummer, E. W. Field emission energy distribution (FEED). *Rev. Mod. Phys.* **1973**, *45*, 487−548.

(58) Bagchi, A.; Gomer, R.; Penn, D. R. Field emission total energy distribution in the presence of adsorbates. *Science* **1974**, *40*, 555−558.

(59) Bell, A. E.; Swanson, L. W. Total energy distributions of field-emitted electrons at high current density. *Phys. Rev. B* **1979**, *19*, 3353−3364.

(60) Lambe, J.; Jaklevic, R. C. Molecular vibration spectra by inelastic electron tunneling. *Phys. Rev.* **1968**, *165*, 821−832.

(61) Lewis, B. F.; Fischer, T. E. Energy distributions of field-emitted electrons from silicon. Evidence for surface states. *Science* **1974**, *40*, 371−376.

(62) Penn, D.; Gomer, R.; Cohen, M. H. Energy distribution in field emission from adsorbate-covered surfaces. *Phys. Rev. Lett.* **1971**, *27*, 26−29.

(63) Lee, T.-H. Ph.D. Thesis, Georgia Insitute of Technology, Atlanta, GA, 2004.

(64) Lee, T.-H.; Hladik, C. R.; Dickson, R. M. Facile, on-demand electronic nanodevice fabrication from photo- and electro-active silver oxide. *Appl. Phys. Lett.* **2004**, *84*, 118−120.

(65) Swanson, L. W.; Crouser, L. C. Effect of polyatomic adsorbates on the total energy distribution of field emitted electrons. *Science* **1970**, *23*, 1−29.

AR040146T